*Desalination and Water Treatment*
www.deswater.com

doi: 10.1080/19443994.2015.1065766

57 (2016) 14696–14707
July

Taylor & Francis
Taylor & Francis Group

# $CuFe_2O_4$@graphene nanocomposite as a sorbent for removal of alizarine yellow azo dye from aqueous solutions

Saeedeh Hashemian*, Maryam Rahimi, Ali Asghar Kerdegari

*Chemistry Department, Islamic Azad University, Yazd Brunch, Yazd, Iran, Tel. +98 31872572; Fax: +98 3537266065; emails: Sa_hashemian@iauyazd.ac.ir (S. Hashemian), rahymi40@gmail.com (M. Rahimi), kerdegari123@gmail.com (A.A. Kerdegari)*

Received 19 January 2015; Accepted 15 June 2015

ABSTRACT

$CuFe_2O_4$@graphene nanocomposite was synthesized by chemical co-precipitation method. The nanocomposite was characterized by Fourier infrared spectroscopy, X-ray diffraction, scanning electron microscopy, and transmission electron microscopy. Adsorption of alizarine yellow (AY) by graphene, $CuFe_2O_4$, and $CuFe_2O_4$@graphene nanocomposite was studied. Effect of different factors including agitation time, pH, and adsorbate concentration on the adsorption capacity of adsorbent for AY dye was investigated. Experimental results demonstrated that AY could be effectively removed from aqueous solution by $CuFe_2O_4$@graphene nanocomposite within 40 min of contact time and pH 3. Two common kinetic models, pseudo-first order and pseudo-second order, were employed to describe the adsorption kinetics. The results indicated that the adsorption kinetics of AY well matched with pseudo-second-order rate expression. The equilibrium adsorption was best described by the Langmuir isotherm model. Various thermodynamic parameters such as the Gibbs free energy ($\Delta G^\circ$), enthalpy ($\Delta H^\circ$), and entropy ($\Delta S^\circ$) change were also evaluated. Thermodynamic results revealed that the adsorption of AY onto $CuFe_2O_4$@graphene is endothermic, spontaneously process and feasible in the range of 303–333 K. The adsorption capacity of $CuFe_2O_4$, graphene, and $CuFe_2O_4$@graphene was found to be 98, 105, and 145 mg $g^{-1}$ for AY, respectively.

*Keywords:* Adsorption; Alizarine yellow; $CuFe_2O_4$@graphene; Nanocomposite

## 1. Introduction

Most of the dyes are toxic and carcinogenic for human health. Various types of dyes are used in the process industries like textile, paints, pulp and paper, carpet and printing, rubber, plastic, leather, cosmetic, pharmaceutical and food industries. The release of wastewaters in the environment is very challenging to aquatic life and mutagenic to human [1]. Therefore, it is important to reduce the dye concentration in the wastewaters before discharging them into the environment. Discharging large amounts of dyes into water resources, accompanied by organics, bleaches, and salts, can affect the physical and chemical properties of fresh water. Alizarin yellow is a mordant dye, suitable for the dyeing of wool and nylon. It is a hazardous azo dye and causes irritation in the eyes, skin, digestive tract, and respiratory tract [2,3]. Investigations are being carried out using different technologies, such as oxidation [4], Fenton-like oxidation [5], ultrasonic [6,7], and adsorption [8–10] for removal of dyes from wastewater. One of the powerful treatment

*Corresponding author.

processes for the removal of dyes from water is adsorption. Adsorption has gained favor in recent years due to proven efficiency in the removal of pollutants from effluents to stable forms. Therefore, adsorption process is one of the effective methods with the advantages of high treatment efficiency and no harmful by-product to treat water. Adsorption techniques have successfully demonstrated on lowering dye concentration from industrial effluents using adsorbents such as activated carbon, clay, and others [11–15]. Activated carbon has been the most widely used adsorbent because of its high capacity for the adsorption of organic species and dyes. However, due to the difficulty and expense involved in regeneration, another sorbents are considered as alternative low-cost absorbent.

Graphene is a kind of novel and interesting carbon material and has attracted tremendous attentions from both the experimental and theoretical scientific communities in recent years [16–18]. Graphene, a new class of two-dimensional carbon nanostructure with one-atom thickness [19,20], receives extensive research interest because of its unique electrical, thermal, mechanical, and optical properties [21,22]. As the large delocalized electron system of graphene can form strong stacking interaction with the benzene ring of dyes [18,19], it might be also a good candidate as an adsorbent for the adsorption of dyes [23]. However, because of its extremely small particle size and high dispersibility in aqueous solution, it is difficult to separate graphene from solution phase after adsorption via traditional centrifugation and filtration. The development of magnetic adsorbents provides a solution to this problem because the magnetic cores ensure the convenient magnetic separation after adsorption. Recently, considerable attention has been focused on the application of magnetic separation technology to solve environmental problems. Magnetic separation is considered as a rapid and effective technique for separating magnetic particles. Magnetic separation, which represents a group of techniques based on the use of magnetic or magnetizable adsorbents, carriers, and cells, has been used for many applications in biochemistry, microbiology, cell biology, analytical chemistry, mining ores, and environmental technologies. Examples of this technology are the use of polymer-coated magnetic particles for oil spill remediation, magnetite particles to accelerate the coagulation of sewage, magnetic $CuFe_2O_4$ powder to adsorb azo-dye acid red B, and magnetic powder $MnFe_2O_4$ composite for the adsorption of organic dyes [24–27]. However, most of these materials have the disadvantage of small adsorption capacity and narrow application range. For example, $CuFe_2O_4$ powder and $MnO–Fe_2O_3$ composite could only be used to adsorb ionic organic pollutants [28]. The graphene-based magnetic nanocomposite was synthesized and its potential practical application in the removal of the dyes and organic compounds from aqueous solution was investigated [29–35].

In this paper, $CuFe_2O_4$@graphene nanocomposite was synthesized and characterized via different methods and used as magnetic adsorbent to remove alizarin yellow (AY) from aqueous solution. Effects of agitation time, initial solution pH, and adsorbate concentration on adsorption of $CuFe_2O_4$@graphene nanocomposite for AY were investigated. The kinetics, thermodynamic, and isotherm of adsorption were also evaluated.

## 2. Experimental

### 2.1. Materials and methods

All chemicals were purchased from Merck chemical co. All compounds were of analytical grade and were used as received without any purification. Distilled water was used in all of the experiments. Alizarin yellow with chemical formula of $C_{13}H_9O_5N_3$ as a sample of pollutant was used. Chemical structure of AY(benzoic acid, 2-hydroxy-5- [(4-nitrophenyl) azo]) is shown in Fig. 1. It has CI Number 14,030 and molecular weight of 309.21 g $mol^{-1}$. The standard solution of 1,000 mg $L^{-1}$ of AY was prepared and subsequently whenever necessary diluted. UV–vis spectrophotometer 160 A Shimadzu was used for the determination of concentration of AY. IR measurements were performed by Fourier infrared spectroscopy (FTIR) tensor-27 of Burker Co., using the KBr pellet between the ranges 400–4,000 $cm^{-1}$. The powder X–ray diffraction studies were made on a Philips PW1840 diffractometer using Ni-filtered Cu kα radiation and wavelength 1.54 Å. The average particle size and morphology of samples were observed by scanning electron microscopy (SEM) using a Hitachi S-3500 SEM. All pH measurements were carried out with an ISTEK- 720P pH meter. Elemental analysis by atomic absorption spectrophotometry was performed on a Shimadzu AA-6800. The prepared $CuFe_2O_4$@graphene showed the 4.32 and 6.56% of Cu and Fe, respectively.

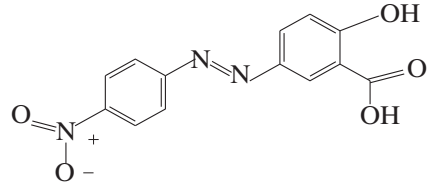


Fig. 1. Chemical structure of AY.

### 2.2. Preparation of graphene oxide

Graphite oxide was prepared from nature graphite powders by a modified Hummers method. Graphene oxide was synthesized by the oxidation of graphite powder using Hummers method [33,34]. Firstly, 120 mL $H_2SO_4$ (95%) was added into a 500 mL flask, and then cooled by immersion in an ice bath followed by stirring. Subsequently, 5.0 g graphite powder and 2.5 g $NaNO_3$ were added under vigorous stirring to avoid agglomeration. After the graphite powder was well dispersed, 15 g $KMnO_4$ was added gradually under stirring, and the temperature of the mixture was kept to be below 10˚C by cooling. The ice bath was then removed and the mixture was stirred at room temperature overnight. As the reaction progressed, the mixture gradually became pasty and the color turned into light brownish. Secondly, 150 mL of $H_2O$ was slowly added to the paste with vigorous agitation. It is because the addition of water in concentrated sulfuric acid medium released a large amount of heat, the addition of water was performed in an ice bath to keep the temperature below 100˚C. The diluted suspension was stirred at 98˚C for 1 d. Then, 50 mL of 30% $H_2O_2$ was added to the mixture. Finally, the mixture was filtered and washed with 5% HCl aqueous solution to remove metal ions followed by water until the pH was 7. After filtration and drying at 65˚C under vacuum, graphene oxide was obtained as gray powder.

### 2.3. Preparation of $CuFe_2O_4$@graphene nanocomposite

The magnetic graphene nanocomposite ($CuFe_2O_4$@-graphene) was synthesized by chemical co-precipitation of $Cu^{2+}$ and $Fe^{3+}$ in alkaline solution in the presence of graphene oxide. The molar ratio of $Cu^{2+}$:$Fe^{3+}$ was 1:2. The magnetic composite was prepared by suspending 0.5 g graphene in 200 mL of solution containing copper (II) chloride ($CuCl_2{\cdot}6H_2O$, 1 mmol) and ferric chloride ($FeCl_3{\cdot}6H_2O$, 2 mmol). The mixture was then titrated dropwise by 1 M $NH_3$ (5%) till the pH was 9 under magnetic stirring at 70˚C. The precipitate was isolated by a permanent magnet. The impurities in the $CuFe_2O_4$@graphene samples were removed by washing with copious amounts of double-distilled water. The prepared sample of $CuFe_2O_4$@graphene was filtered off, washed with distilled water, and then dried in a furnace at 300˚C for 3 h [10,11]. $CuFe_2O_4$ was prepared as the same method without graphene oxide.

### 2.4. Adsorption experiments

Different parameters like contact time, adsorbent dosage, and pH on the sorption capacity of AY have been studied. The removal of AY dye from aqueous solutions by sorbents was carried out using following experimental procedures:

The initial dye concentration in each sample was 50 mg $L^{-1}$. 0.5 g of sorbent was added in 30 ml sample on rotary shaker at a constant speed of 300 rpm. All experiments were conducted at 25˚C. After different contact times (0–360 min), the sorbent was removed from the solution and the equilibrium concentration of the dye in the solution was determined with UV spectrophotometer at the wavelength 370 nm ($\lambda_{max}$). To optimize the adsorbent dosage, different doses of the sorbents were examined. A known amount of sorbent (0.05–3 g) was added to 30 mL of dye solutions in the concentration range from 20 to 60 mg $L^{-1}$. The influence of the solution pH on the dye removal was also studied by adding a certain amount of the sorbent into the dye solutions with the pH of the solution being adjusted from 2 to 10 with 0.1 mol $L^{-1}$ HCl or 0.1 mol $L^{-1}$ NaOH. The remaining concentration of the dye in the solution was then determined by UV–vis spectrometry and the relative dye adsorption (%) vs. adsorption time was determined. The percent removal of AY by the hereby adsorbent is given by:

$$\% \text{ Removal} = (C_0 - C_e)/C_0 \times 100$$

where $C_0$, $C_e$ denotes the initial and equilibrium concentration (mg $L^{-1}$) of AY, respectively. The removed quantity ($q_e$ in mg $L^{-1}$) of the dye by sorbent was calculated by where $C_0$ (mg $L^{-1}$) represents the initial dye concentration, $C_e$ (mg $L^{-1}$) is the equilibrium concentration of the dye remaining in the solution, $V$ (L) is the volume of the aqueous solution, and $m$ (g) is the weight of the sorbent.

$$q_e = (C_0 - C_e)V/m$$

### 2.5. Desorption studies

For desorption study, 1 g of $CuFe_2O_4$@graphene nanocomposite was added to 50 mL of the dye solution 60 mg $L^{-1}$ and the mixture was shaken on a rotary shaker at 300 rpm for 1 h. At the end of the adsorption, the dye-adsorbed $CuFe_2O_4$@graphene was isolated from the mixture with a magnet and then calcined at different temperatures. Then the supernatant solution was analyzed by UV–vis spectrometry. Desorption efficiency of the dye from the $CuFe_2O_4$@graphene adsorbent was calculated as the ratio of the amount of the dye desorbed to amount of the dye adsorbed.

## 3. Results and discussion

### 3.1. Characterization of sorbents

The FTIR spectra of graphite, graphene oxide, $CuFe_2O_4$, and $CuFe_2O_4$@graphene nanocomposite are shown in Fig. 2(a)–(d). No significant peak was found in graphite (Fig. 2(a)). Graphene oxide and $CuFe_2O_4$@graphene nanocomposite both showed the OH stretching vibration adsorption peaks at 3,400 and 1,622 $cm^{-1}$ (Fig. 2(b) and (d)). The presence of different types of oxygen is shown in GO (Fig. 2(b)). As to $CuFe_2O_4$@graphene (Fig. 2(d)), the peak at 1,384 $cm^{-1}$ is assigned to the C=O stretching vibration and the peak at 1,077 $cm^{-1}$ is ascribed to the C–O stretching vibration of epoxy group and alkoxy. These peaks demonstrated the existence of carboxyl, epoxy group, and alkoxy in graphene oxide. $CuFe_2O_4$@graphene nanocomposite exhibited a new peak at 1,360–1,384 $cm^{-1}$. The Fe–O and Cu–O characteristic stretching vibration peaks were observed at 608 and 485 $cm^{-1}$ in curve *d*, which confirmed that $CuFe_2O_4$ nanoparticles were successfully anchored onto graphene sheet [36,37].

X-ray diffraction (XRD) measurements were employed to investigate the phase and structure of the synthesized samples. Fig. 3 shows the XRD of graphite, graphene oxide, $CuFe_2O_4$, and $CuFe_2O_4$@graphene nanocomposites. As shown in Fig. 3, the XRD pattern of graphite (Fig. 3(a)) shows a broad peak at $2\theta = 26.2^\circ$ corresponding to the hexagonal lattice of (0 0 2) plane with 3.36 Å spacing between the layers, which agrees well with the lattice plane reported in the JCPDS (No. 04-0783). After oxidation of graphite to graphene oxide, the peak at $2\theta = 26.2^\circ$ disappeared and a new peak at $2\theta = 11.2^\circ$ corresponding to (0 0 1) plane and layer distance of 8.1 Å was observed (Fig. 3(b)). XRD of $CuFe_2O_4$ is shown in Fig. 3(c). From Fig. 3(d) ($CuFe_2O_4$@graphene) new significant diffraction peaks ($2\theta = 32.5^\circ$ (2 2 0), $35.6^\circ$ (3 1 1), $43.5^\circ$ (4 0 0), and $62.8^\circ$ (4 4 0)) can be assigned to the crystal planes of $CuFe_2O_4$. $CuFe_2O_4$@graphene shows the spinel structure. All of the new significant diffraction peaks of the $CuFe_2O_4$@graphene sample matched well with the data from the JCPDS cards (19-0629) and (74-2403). In the XRD pattern of $CuFe_2O_4$@graphene, peak at $2\theta = 11.2^\circ$ disappeared. It is due to the reduction of graphene oxide to graphene nanosheets and detachment of oxygen groups. The particle size from Schere's equation ($t = K\lambda/\beta \cos\theta$) that is the average size of the particles. From the $\beta$ (the full width at half maximum of the diffracted peak) and $\theta$, the angle of diffraction of $CuFe_2O_4$@graphene is calculated about 30–60 nm for different particles.

The SEM images of graphene oxide, $CuFe_2O_4$, and $CuFe_2O_4$@graphene composite are shown in Fig. 4a((a)–(c)). It can be clearly seen that the crumpled silk waves-like carbon sheets exist, a characteristic feature of the single-layer graphene sheets (Fig. 4a). As shown in Fig. 4, the $CuFe_2O_4$ nanoparticles were successfully coated on the surface of graphene oxide to form $CuFe_2O_4$@graphene nanocomposite. The $CuFe_2O_4$ nanoparticles were well distributed on graphene sheets, which were nearly flat and had a big area up to several square micrometers. Some nanoparticles were slightly aggregated due to the close to saturation loading degree. Energy dispersion

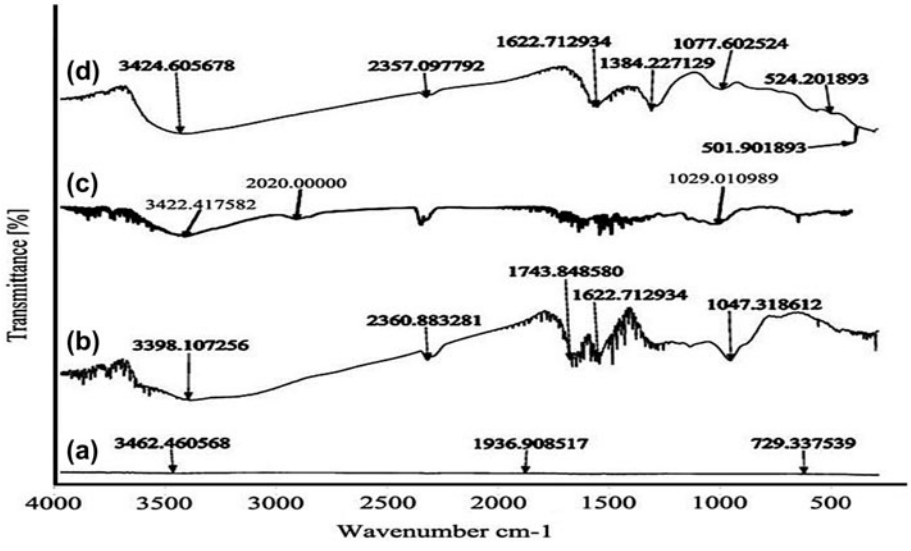


Fig. 2. FTIR spectra of (a) graphite, (b) graphene oxide, (c) $CuFe_2O_4$, and (c) $CuFe_2O_4$@graphene nanocomposite.

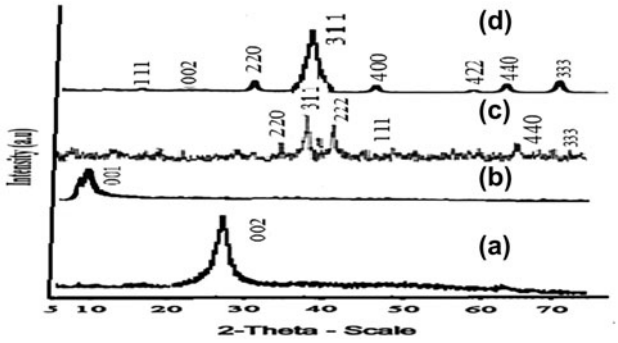


Fig. 3. The XRD pattern of (a) graphite, (b) graphene oxide, (c) $CuFe_2O_4$, and (d) $CuFe_2O_4$@graphene nanocomposite.

X-ray (EDX) and transmission electron microscopy (TEM) image of $CuFe_2O_4$@graphene nanocomposite is shown in Fig. 4b((a) and (b)), respectively. From TEM image of $CuFe_2O_4$@ graphene nanoparticles, average particle size 50 nm was observed.

### 3.2. Adsorption study

#### 3.2.1. Effect of contact time

Effect of contact time on the adsorption of AY onto $CuFe_2O_4$, graphene oxide, and $CuFe_2O_4$@graphene nanoparticles was investigated at different times (0–360 min). 30 mL of 60 mg $L^{-1}$ of AY with 0.5 g of each sorbent with 300 rpm were contacted. After different agitation times, absorbance of filtrated dye was determined. The differences of absorbance before and after adsorption onto sorbents showed the percent of AY removal. It was found that more than 70% removal of AY occurred in the first 40 min, and thereafter the rate of adsorption was found to be slow. The percent of adsorption of AY as a function of time is shown in Fig. 5. It is obvious that $CuFe_2O_4$@graphene nanoparticles have the highest rate than $CuFe_2O_4$ and graphene oxide for removal of AY dye. It is due to the catalytic activity of $CuFe_2O_4$ onto graphene sheets.

#### 3.2.2. Effect of initial solution pH

The percentage of AY adsorption was studied as a function of pH in the range of 2–10. For studying effect of pH on adsorption of AY by $CuFe_2O_4$, graphene, and $CuFe_2O_4$@graphene, initial concentration of dye solutions of 60 mg $L^{-1}$ were treated by 0.5 g adsorbent for 40 min with varying pH 2–10. For maintain pH 0.01 M HCl and 0.01 M NaOH solutions were used. Point zero charge is a useful factor in sorption studies that allows one to hypothesize on the ionization of functional groups and their interactions with adsorbates [38]. The pH of zero net proton charge is defined here as the pH value at which the net surface charges is equal to zero. The point of zero charge of graphene and $CuFe_2O_4$@-graphene nanocomposite was measured. Both of graphene and $CuFe_2O_4$@graphene nanocomposite showed the point of zero charge 3.1 and 3.3, respectively. Fig. 6 displays the effect of pH on the removal percentage of AY by $CuFe_2O_4$, graphene oxide, and $CuFe_2O_4$@-graphene. It was observed that the dye adsorbed increased when pH was increased to 3, and then was not significantly altered. At $pH < pH_{pzc}$, sorbent surface has positive charged. AY is azo anionic dye, which exists in aqueous solution in the form of negative-charged ions. At lower pH values, due to the protonation of the hydroxyl groups, AY can be ionized and consequently increases its electrostatic force of attraction with sorbent. Adsorption of AY decreased with increasing pH from 4 to 10.

#### 3.2.3. Effect of adsorbent mass

The effect of the adsorbent dose on the removal of the AY was studied by varying the amount of

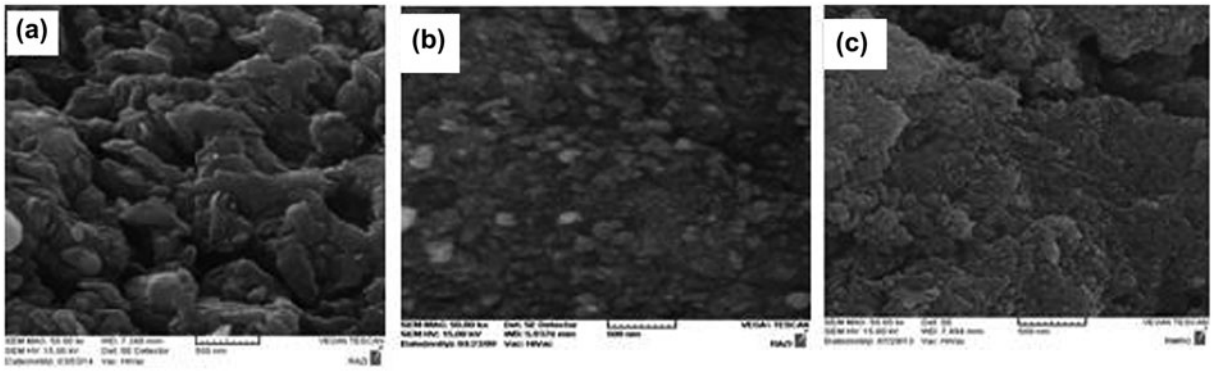


Fig. 4a. SEM image of (a) graphene oxide, (b) $CuFe_2O_4$, and (c) $CuFe_2O_4$@graphene nanocomposite.

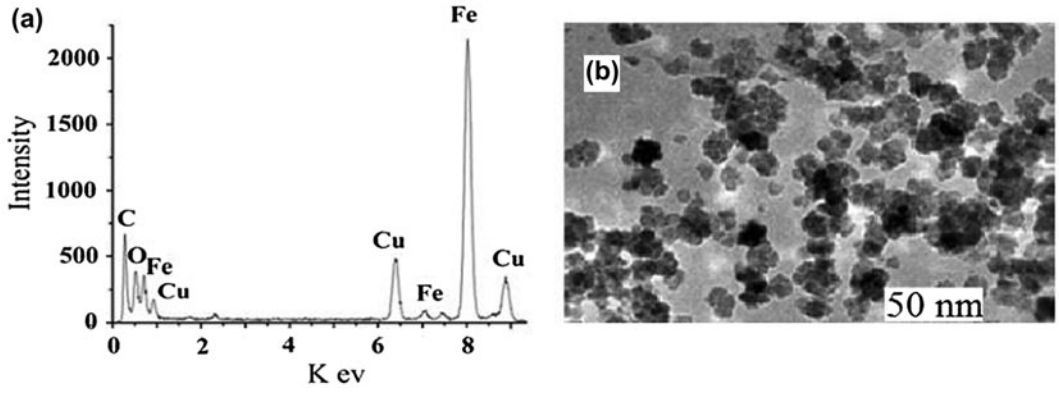


Fig. 4b. (a) EDX and (b) TEM image of $CuFe_2O_4$@graphene nanocomposite.

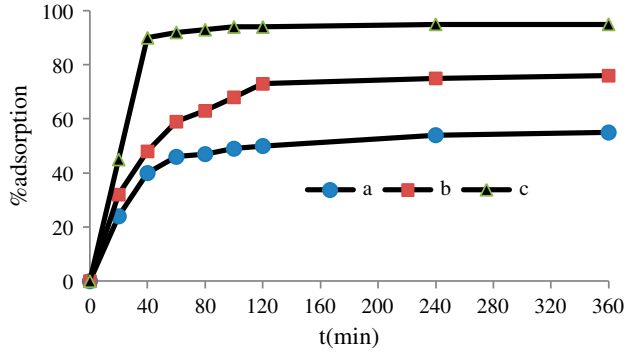


Fig. 5. Effect of contact time on the adsorption of AY onto (a) $CuFe_2O_4$, (b) graphene oxide, and (c) $CuFe_2O_4$@-graphene nanocomposite.

adsorbent from 0.01 to 3 g. It was observed that the amount of dye adsorbed varied with varying adsorbent mass and increased with increasing adsorbent mass. The effect of different adsorbent dosages within the range 0.01–3 g on the removal of AY by $CuFe_2O_4$, graphene oxide, and $CuFe_2O_4$@graphene nanocomposite is shown in Fig. 7. It is seen that the percentage removal of AY initially increased rapidly to more than 95% as the $CuFe_2O_4$@graphene amount was increased up to 0.5 g, which may be attributed to the greater availability of adsorption sites with increasing amounts of $CuFe_2O_4$@graphene nanocomposite. The alizarin removal efficiency increased up to 63% for graphene. It is evident that the number of available adsorption points increases at high adsorbent quantity and therefore leads to an increase in the amount of removed AY. The removal more than 0.5 g of adsorbent dosage is only marginal. However, after the attainment of a critical dosage (0.5 g), the percentage removal of AY was slowly increased.

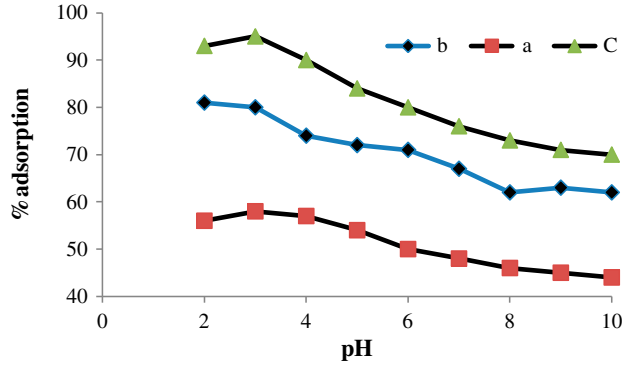


Fig. 6. Effect of pH of solutions on the adsorption of AY by (a) $CuFe_2O_4$, (b) graphene oxide, and (c) $CuFe_2O_4$@-graphene nanocomposite.

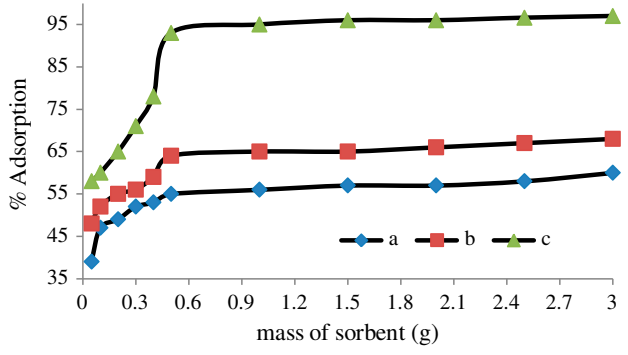


Fig. 7. Effect of sorbent dosage on the adsorption of AY by (a) $CuFe_2O_4$, (b) graphene oxide, and (c) $CuFe_2O_4$@-graphene nanocomposite.

### 3.2.4. Influence of ionic strength

The influence of ionic strength on the removal of AY by $CuFe_2O_4$@graphene was investigated with the NaCl and $Na_2SO_4$ concentration over the range from 0 to 20% (w/v). As a result, no significant influence of ionic strength on the removal of the dye was observed. The independence of the sodium salts concentration on dye adsorption is important for the application of $CuFe_2O_4$@graphene in the removal of some organic pollutants from wastewaters since the salt concentration may be different in different samples [29].

## 3.3. Adsorption kinetics

Adsorption kinetics which provides the information about adsorption path and adsorption mechanism could evaluate adsorption performance of the adsorbent. In the present study, the kinetic data of the adsorption of AY by $CuFe_2O_4$, graphene oxide, and $CuFe_2O_4$@graphene were evaluated using pseudo-first-order [39] and pseudo-second-order [40] kinetic models. The pseudo-first-order model assumes that the rate of change of solute uptake with time is directly proportional to the difference in saturation concentration and amount of solid uptake with time [39].

$$\ln(q_e - q_t) = \ln q_e - k_1 t \quad (1)$$

where $q_e$ and $q_t$ are the amounts of dye adsorbed per unit mass of the adsorbent (mg $g^{-1}$) at equilibrium and time $t$, respectively, and $k_1$ is the rate constant of adsorption ($min^{-1}$). When ln $(q_e - q_t)$ was plotted against time, a straight line should be obtained with a slope of $k_1$, if the first-order kinetics is valid.

The pseudo-second-order model as developed by Ho and McKay [40] has the following form:

$$t/q_t = t/q_e + 1/(k_2 q_e^2) \quad (2)$$

where $q_e$ and $q_t$ represent the amount of dye adsorbed (mg $g^{-1}$) at equilibrium and at any time. $k_2$ in the rate constant of the pseudo-second-order equation (g $mg^{-1}$ $min^{-1}$). A plot of $t/q$ vs. time ($t$) would yield a line with a slope of $1/q_e$ and an intercept of $1/(k_2 q_e^2)$, if the second-order model is a suitable expression.

The plot between ln $(q_e - q_t)$ vs. time $t$ shows the pseudo-first-order model and the plot of $t/q$ vs. time $t$ shows the pseudo-second-order model (Figs. 8 and 9), respectively. The kinetic model with a higher correlation coefficient $R^2$ was selected as the most suitable one (Table 1). The results show that the adsorption

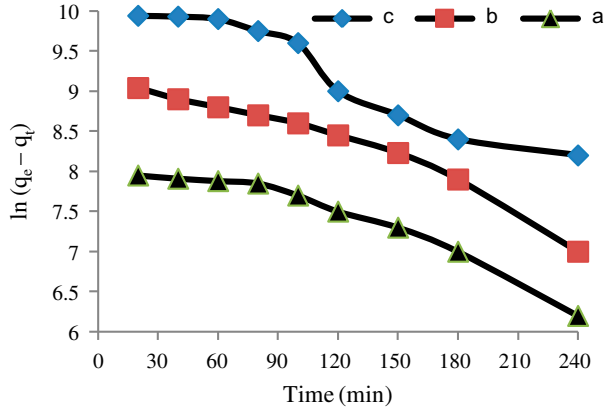


Fig. 8. Pseudo-first-order kinetic model for adsorption of AY onto (a) $CuFe_2O_4$, (b) graphene oxide, and (c) $CuFe_2O_4$@graphene nanocomposite.

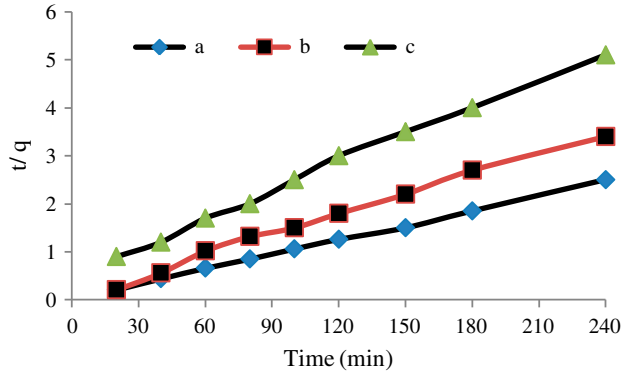


Fig. 9. Pseudo-second-order kinetic model for adsorption of AY onto (a) $CuFe_2O_4$, (b) graphene oxide, and (c) $CuFe_2O_4$@graphene nanocomposite.

kinetics of AY fitted well with the pseudo-second-order kinetic model.

The results are shown in Table 1. The adsorption of AY onto $CuFe_2O_4$@graphene nanocomposite was followed by pseudo-second-order kinetic model. It could be concluded that the chemical interaction might be involved in the adsorption process.

## 3.4. Adsorption isotherm

Adsorption capacity and adsorption behavior of AY on $CuFe_2O_4$@graphene nanocomposite can be illustrated by adsorption isotherm. Data from the adsorption isotherms were modeled using the Langmuir and Freundlich isotherm models and the resulting isotherm constants are presented in Table 2. The Langmuir theory was valid for monolayer adsorption

Table 1
Kinetics parameters for the removal of AY onto $CuFe_2O_4$, graphene oxide, and $CuFe_2O_4$@graphene nanocomposite

| | First order | | Second order | |
|---|---|---|---|---|
| Sample | $R^2$ | $K_1(s^{-1})$ | $R^2$ | $K_2$(g mg$^{-1}$ min$^{-1}$) |
| $CuFe_2O_4$ | 0.921 | $7 \times 10^{-3}$ | 0.998 | 0.0625 |
| Graphene | 0.942 | $8 \times 10^{-3}$ | 0.992 | 0.230 |
| $CuFe_2O_4$@graphene | 0.926 | $9 \times 10^{-3}$ | 0.996 | 1.534 |

onto a surface containing a finite number of identical adsorption sites and there is no important interaction between the adsorbate molecules adsorbed on the adjacent adsorption sites of the adsorbent. Langmuir isotherm theory is based on the assumption of adsorption on a homogeneous surface. The Langmuir equation can be written in the following form:

$$C_e/q_e = (1/q_{max}k_L) + C_e/q_{max} \quad (3)$$

where $q_e$ is the solid phase equilibrium concentration (mg g$^{-1}$), $C_e$ is the liquid equilibrium concentration of dye in solution (mg L$^{-1}$), $k_L$ is the equilibrium adsorption constant related to the affinity of binding sites (L mg$^{-1}$), and $q_{max}$ is the maximum amount of the dye per unit weight of adsorbent for complete monolayer coverage.

The Freundlich isotherm model is an empirical theory available for heterogeneous surface possessing sites with different sorption energy, which suggested that the adsorption capacity is related to the equilibrium concentration of the adsorbate. The Freundlich isotherm describes adsorption where the adsorbent has a heterogeneous surface with adsorption sites that have different energies of adsorption. The energy of adsorption varies as a function of the surface coverage ($q_e$) and is represented by the Freundlich constant $K_F$ (l g$^{-1}$) in Eqs. (4) and (5).

$$q_e = K_F C_e^{1/n} \quad (4)$$

$$\log q_e = \log K_F + 1/n \log C_e \quad (5)$$

where $K_F$ is roughly an indicator of the adsorption capacity and $n$ is the heterogeneity factor which has a lower value for more heterogeneous surfaces. As seen in Table 2, AY adsorption onto the $CuFe_2O_4$@graphene nanocomposite was well described by the Langmuir model with correlation coefficients of $R^2 = 0.995$. The maximum adsorption capacity $q_{max}$ was 145 mg g$^{-1}$. Results from the Freundlich analysis shown in Table 2 indicate that the correlation coefficient is significantly less than the Langmuir analysis in describing the adsorption of AY. The fact that the Langmuir isotherm fits the experimental data very well may be due to homogenous distribution of active sites on the $CuFe_2O_4$@graphene composite surface. Results from the Langmuir and Freundlich analysis of the adsorption of AY on the $CuFe_2O_4$@graphene nanocomposite are also reported in Table 2. The fitting curves and correlation coefficient values both indicate that the Langmuir model describes better the adsorption onto $CuFe_2O_4$@graphene composite.

### 3.5. Thermodynamic studies

The thermodynamic parameters, change in the standard free energy ($\Delta G^\circ$), enthalpy ($\Delta H^\circ$), and entropy ($\Delta S^\circ$) associated with the adsorption process and these were determined using the following equations [41]:

$$\Delta G^\circ = -RT \ln K_C \quad (6)$$

Table 2
Langmuir and Freundlich isotherm constants for adsorption of AY onto graphene oxide, $CuFe_2O_4$, and $CuFe_2O_4$@graphene nanocomposite

| | Freundlich | | | Langmuir | | |
|---|---|---|---|---|---|---|
| Sorbent | $K_F$ | $n$ | $R^2$ | $q_m$ (mg g$^{-1}$) | $K_L$ (L mg$^{-1}$) | $R^2$ |
| Graphene | 15.91 | 2.25 | 0.951 | 105 | 34.62 | 0.9657 |
| $CuFe_2O_4$ | 2.07 | 4.07 | 0.927 | 98 | 75.2 | 0.9849 |
| $CuFe_2O_4$@graphene | 0.25 | 4.79 | 0.940 | 145 | 5.7 | 0.995 |

Table 3
Thermodynamic parameters for adsorption of AY by adsorption onto graphene oxide, $CuFe_2O_4$, and $CuFe_2O_4$@graphene nanocomposite

| Sample | $T$ (K) | $\Delta G^\circ$ (kJ mol$^{-1}$) | $\Delta H^\circ$ (kJ mol$^{-1}$) | $\Delta S^\circ$ (J mol$^{-1}$ k$^{-1}$) |
|---|---|---|---|---|
| Graphene | 303 | −15.13 | 102.47 | 53.86 |
| | 313 | −15.80 | | |
| | 323 | −16.31 | | |
| | 333 | −16.82 | | |
| $CuFe_2O_4$ | 303 | −15.06 | 227.04 | 50.99 |
| | 313 | −15.73 | | |
| | 323 | −16.25 | | |
| | 333 | −16.75 | | |
| $CuFe_2O_4$@graphene | 303 | −15.66 | 2,213.76 | 59.75 |
| | 313 | −16.52 | | |
| | 323 | −17.12 | | |
| | 333 | −17.68 | | |

where $\Delta G^\circ$ is the standard free energy change, $T$ is the absolute temperature, $R$ is the universal gas constant (8.314 J mol$^{-1}$ K$^{-1}$), and $K_C$ is the equilibrium constant. The apparent equilibrium constant of the sorption, $K_C$, is obtained from:

$$K_C = C_A/C_S \quad (7)$$

where $K_C$ is the equilibrium constant, $C_A$ is the amount of AY adsorbed on the adsorbent of solution at equilibrium (mg L$^{-1}$), $C_S$ is the equilibrium concentration of AY in the solution (mg L$^{-1}$). $K_C$ values calculated at different temperatures allow the determination of the thermodynamic equilibrium constant ($K_C$) [41]. The free energy changes are also calculated using the following equations:

$$\ln K_C = -\Delta G^\circ/RT = -\Delta H^\circ/RT + \Delta S^\circ/R \quad (8)$$

$\Delta H^\circ$ and $\Delta S^\circ$ were calculated, the slope and intercept of van t Hoff plots of ln $K_C$ vs. $1/T$. The results of thermodynamic parameters of AY adsorption onto graphene oxide, $CuFe_2O_4$, and $CuFe_2O_4$@graphene nanocomposite are given in Table 3.

### 3.6. Comparison of $CuFe_2O_4$@graphene nanocomposite with other adsorbents

The adsorption capacity of AY onto $CuFe_2O_4$@graphene nanocomposite was compared with several other adsorbents and they are reported in Table 4. $CuFe_2O_4$@graphene nanocomposite in this study possesses reasonable adsorption capacity in comparison with other sorbents.

### 3.7. Regeneration of the spent composites

The adsorption capacity of the $CuFe_2O_4$@graphene nanocomposite for AY after its regeneration has also

Table 4
Comparison of maximum adsorption capacities of alizarin dyes with different sorbents

| No. | Dye | $q_{max}$ (mg L$^{-1}$) | Absorbent | References |
|---|---|---|---|---|
| 1 | Alizarin Yellow | 93.29 | *Casuarina equisetifolla* | [42] |
| 2 | Alizarin Yellow | 75.44 | Charcoal | [43] |
| 3 | Alizarin Red-S | 94.67 | *Abelmoschus esculentus* stem powder | [44] |
| 4 | Alizarin Red-S | 84.4 | ZnO and $TiO_2$ | [45] |
| 5 | Alizarin Red | 91.04 | Ultra-fine fly ash | [46] |
| 6 | Alizarin Red-S | 95 | Cynodon dactylon | [47] |
| 7 | Alizarin Red-S | 78 | Nanosized silica modified | [48] |
| 8 | Alizarin Red-S | 83 | Nanocrystalline $Cu_{0.5}Zn_{0.5}Ce_3O_5$ | [49] |
| 9 | Alizarin Red-S | 95.74 | Citrullus lanatus peels | [50] |
| 10 | Alizarin Yellow | 145 | $CuFe_2O_4$@graphene | In this study |
| 11 | Alizarin Yellow | 98 | $CuFe_2O_4$ | In this study |
| 12 | Alizarin Yellow | 105 | Graphene oxide | In this study |

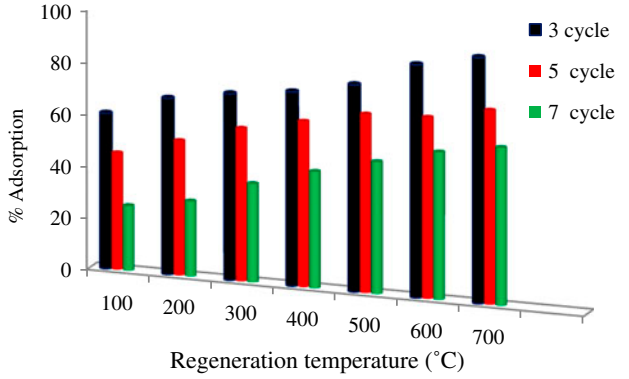


Fig. 10. Effect of physical desorption of AY onto $CuFe_2O_4$@graphene nanocomposite.

been studied. The spent composite was regenerated following the process mentioned below. The regenerated samples were again saturated with AY with the same initial concentration of 60 mg $L^{-1}$ and then determined their new adsorption capacity. The physically regeneration of adsorbent was done by heated $CuFe_2O_4$@graphene nanocomposite adsorbed AY at 100–700°C. These adsorption–regeneration cycles were carried out 3, 5, and 7 times. The regenerated $CuFe_2O_4$@graphene nanocomposite was reused for the adsorption experiments. The adsorption capacity of the $CuFe_2O_4$@graphene nanocomposite for AY did not show any significant decrease even after three regenerations. After five cycle 90% and after seven cycle 62% of AY was removed. The obtained results are shown in Fig. 10. The value of cycle corresponds to the adsorption capacity of the original composite. Generally, the adsorption capacity of the composite decreased as the number of regeneration cycle increased.

## 4. Conclusion

In this study, $CuFe_2O_4$@graphene nanocomposite adsorbent has been prepared to successfully remove the AY azo organic dye from aqueous solutions. Effects of different conditions on adsorption of AY onto graphene oxide, $CuFe_2O_4$, and $CuFe_2O_4$@-graphene nanocomposite were investigated. Experimental results demonstrated $CuFe_2O_4$@graphene nanocomposite could effectively remove AY from aqueous solution within 40 min. The adsorption process was very fast and reached the adsorption equilibrium with 40 min of contact time. Kinetic data were well fitted by a pseudo-second-order model. Langmuir and Freundlich models were used to study the adsorption isotherms. The results showed that the $CuFe_2O_4$@graphene can be used as an effective adsorbent for simple and rapid removal of AY from aqueous. $CuFe_2O_4$@graphene nanocomposite could be conveniently regenerated after adsorption.

## Acknowledgments

The authors wish to thank Islamic Azad University of Yazd (IAUY) for the financial support of this work. Also, thank co-workers and technical staff in the chemical department help during various stages of this work.

## References

[1] S.L. Marco, J.A. Peres, Decolorization of the azo dye reactive black 5 by Fenton and Photo-Fenton oxidation, Dyes Pigment 71 (2006) 236–244.
[2] Z.S. Seddigi, Removal of alizarin yellow dye from water using zinc doped $WO_3$ catalyst, Bull. Environ. Contam. Toxicol. 84(5) (2010) 564–567.
[3] K. Hayat, M.A. Gondal, M.M. Khaled, S. Ahmed, Kinetic study of laser-induced photocatalytic degradation of dye (alizarin yellow) from wastewater using nanostructured ZnO, J. Environ. Sci. Health. A Tox. Hazard. Subst. Environ. Eng. 45(11) (2010) 1413–1420.
[4] L. Szpyrkowicz, C. Juzzolino, S.N. Kaul, A comparative study on oxidation of disperse dyes by electrochemical process, ozone, hypochlorite and Fenton reagent, Water Res. 35(9) (2001) 2129–2136.
[5] S. Hashemian, Fenton-like oxidation of malachite green solutions: Kinetic and thermodynamic study, J. Chem. (2013) 1–7 (Article ID 809318), doi: 10.1155/2013/809318.
[6] M. Roosta, M. Ghaedi, A. Daneshfar, S. Darafarin, R. Sahraei, M.K. Purkait, Simultaneous ultrasound-assisted removal of sunset yellow and erythrosine by ZnS: Ni nanoparticles loaded on activated carbon: Optimization by central composite design, Ultrason. Sonochem. 21(4) (2014) 1441–1450.
[7] M. Roosta, M. Ghaedi, A. Daneshfar, R. Sahraei, A. Asghari, Optimization of the ultrasonic assisted removal of methylene blue by gold nanoparticles loaded on activated carbon using experimental design methodology, Ultrason. Sonochem. 21(1) (2014) 242–252.
[8] A. Mittal, V. Thakur, J. Mittal, H. Vardhan, Process development for the removal of hazardous anionic azo dye Congo red from wastewater by using hen feather as potential adsorbent, Desalin. Water Treat. 52(1–3) (2014) 227–237.
[9] V.K. Gupta, Suhas, Application of low-cost adsorbents for dye removal—A review, J. Environ. Manage. 90(8) (2009) 2313–2342.
[10] S. Hashemian, M. Salimi, Nano composite a potential low cost adsorbent for removal of cyanine acid, Chem. Eng. J. 188 (2012) 57–63.
[11] M. Ghaedi, A. Ansari, M.H. Habibi, A.R. Asghari, Removal of malachite green from aqueous solution by zinc oxide nanoparticle loaded on activated carbon: Kinetics and isotherm study, J. Ind. Eng. Chem. 20 (2014) 17–28.

[12] G. Crini, Non-conventional low-cost adsorbents for dye removal: A review, Bioresour. Technol. 97 (2006) 1061–1085.
[13] S. Hashemian, M. Monshizadeh, Removal of methylene blue from aqueous solution by nano $LaFeO_3$ particles, Main Group Chem. 12 (2013) 113–124.
[14] R. Jain, P. Sharma, S. Sikarwar, J. Mittal, D. Pathak, Adsorption kinetics and thermodynamics of hazardous dye Tropaeoline 000 unto Aeroxide Alu C (Nano alumina): A non-carbon adsorbent, Desalin. Water Treat. 52(40–42) (2014) 7776–7783.
[15] V. Vimonses, B. Jin, C.W.K. Chow, C. Saint, Enhancing removal efficiency of anionic dye by combination and calcination of clay materials and calcium hydroxide, J. Hazard. Mater. 171 (2009) 941–947.
[16] K.S. Novoselov, A.K. Geim, S.V. Morozov, D. Jiang, Y. Zhang, S.V. Dubonos, I.V. Grigorieva, A.A. Firsov, Electric field effect in atomically thin carbon films, Science 306 (2004) 666–669.
[17] R.F. Service, Carbon sheets an atom thick give rise to graphene dreams, Science 324 (2009) 875–877.
[18] M.J. Allen, V.C. Tung, R.B. Kaner, Honeycomb carbon: A review of graphene, Chem. Rev. 110 (2010) 132–145.
[19] D.R. Dreyer, S. Park, C.W. Bielawski, R.S. Ruoff, The chemistry of graphene oxide, Chem. Soc. Rev. 39 (2010) 228–240.
[20] Y.B. Luo, J.S. Cheng, Q. Ma, Y.Q. Feng, J.H. Li, Graphene–polymer composite: Extraction of polycyclic aromatic hydrocarbons from water samples by stir rod sorptive extraction, Anal. Methods 3 (2011) 92–98.
[21] J.M. Chen, J. Zou, J.B. Zeng, X.H. Song, J.J. Ji, Y.R. Wang, J. Ha, X. Chen, Preparation and evaluation of graphene-coated solid-phase microextraction fiber, Anal. Chim. Acta 678 (2010) 44–49.
[22] X.P. Shen, J.L. Wu, S. Bai, H. Zhou, One-pot solvothermal syntheses and magnetic properties of graphene-based magnetic nanocomposites, J. Alloys Compd. 506 (2010) 136–140.
[23] P. Sharma, M.R. Das, Removal of a cationic dye from aqueous solution using graphene oxide nanosheets: Investigation of adsorption parameters, J. Chem. Eng. Data 58(1) (2013) 151–158.
[24] M. Ghaedi, S. Hajjati, Z. Mahmudi, I. Tyagi, S. Agarwal, Modeling of competitive ultrasonic assisted removal of the dyes – methylene blue and safranin-O using $Fe_3O_4$ nanoparticles, Chem. Eng. J. 268 (2015) 28–37.
[25] W. Rongcheng, Q. Jiuhum, H. Hong, Y. Yunbo, Removal of azo-dye acid red B (ARB) by adsorption and catalytic combustion using magnetic $CuFe_2O_4$ powder, Appli. Catal., B 48 (2004) 46–56.
[26] L. Wang, J. Li, Y. Wang, L. Zhao, Q. Jiang, Adsorption capability for Congo red on nanocrystalline $MFe_2O_4$ (M=Mn, Fe, Co, Ni) spinel ferrites, Chem. Eng. J. 181–182 (2012) 72–79.
[27] S. Hashemian, Removal of acid red 151 from water by adsorption onto nano-composite $MnFe_2O_4$/kaolin, Main Group Chem. 10 (2011) 105–114.
[28] G. Zhang, J. Qu, H. Liu, A.T. Cooper, R. Wu, $CuFe_2O_4$/activated carbon composite: A novel magnetic adsorbent for the removal of acid orange II and catalytic regeneration, Chemosphere 68 (2007) 1058–1066.
[29] C. Wang, C. Feng, Y. Gao, X. Ma, Q. Wu, Z. Wang, Preparation of a graphene-based magnetic nanocomposite for the removal of an organic dye from aqueous solution, Chem. Eng. J. 173 (2011) 92–97.
[30] F.A. He, J.T. Fan, D. Ma, L.M. Zhang, C. Leung, H.L. Chan, The attachment of $Fe_3O_4$ nanoparticles to graphene oxide by covalent bonding, Carbon 48 (2010) 3139–3144.
[31] J.F. Shen, Y.Z. Hu, M. Shi, N. Li, H.W. Ma, M.X. Ye, One step synthesis of graphene oxide-magnetic nanoparticle composite, J. Phys. Chem. C 114 (2010) 381498–381503.
[32] Y.P. Chang, C.L. Ren, J.C. Qu, X.G. Chen, Preparation and characterization of $Fe_3O_4$/graphene nanocomposite and investigation of its adsorption performance for aniline and p-chloroaniline, Appl. Sur. Sci. 261 (2012) 504–509.
[33] W.S. Hummers, R.E. Offeman, Preparation of graphitic oxide, J. Am. Chem. Soc. 80 (1958) 1339–1339.
[34] X. Yang, X. Zhang, Y. Ma, Y. Huang, Y. Wang, Y. Chen, Superparamagnetic graphene oxide–$Fe_3O_4$ nanoparticles hybrid for controlled targeted drug carriers, J. Mater. Chem. 19 (2009) 2710–2714.
[35] T. Kuilla, S. Bhadra, D.H. Yao, N. Kim, S. Bose, J. Lee, Recent advances in graphene based polymer composites, Prog. Poly. Sci. 35(11) (2010) 1350–1375.
[36] L. Zheng, G. Zhang, M. Zhang, S. Guo, Z.H. Liu, Preparation and capacitance performance of Ag–graphene based nanocomposite, J. Power Sources 201 (2012) 376–381.
[37] D. Li, M.B. Müller, S. Gilje, R.B. Kaner, G.G. Wallace, Processable aqueous dispersions of graphene nanosheets, Nat. Nanotechnol. 3(2) (2008) 101–105.
[38] M. Ghaedi, M. Montazerozohori, M. Nejati Biyareh, K. Mortazavi, M. Soylak, Chemically bonded multiwalled carbon nanotubes as efficient material for solid phase extraction of some metal ions in food samples, Int. J. Environ Anal. Chem. 93(5) (2013) 528–542.
[39] S. Lagergren, About the theory of so-called adsorption of soluble substances, Kungliga Svenska Vetenskapsakademiens Handlingar 24 (1898) 1–39.
[40] Y.S. Ho, G. McKay, The kinetics of sorption of basic dyes from aqueous solution by sphagnum moss peat, Canadian J. Chem. Eng. 76 (1998) 822–827.
[41] S. Hashemian, M. Mirshamsi, Kinetic and thermodynamic of adsorption of 2-picoline by sawdust from aqueous solution, J. Ind. Eng. Chem. 18 (2012) 2010–2015.
[42] P.M. Devaprasath, J.S. Solomon, Adsorption modeling of alizarin yellow on biosorbent casuarina equisetifolla, Int. J. Res. Chem. Environ. 2 (2011) 201–212.
[43] M. Salman, M. Athar, U. Shafique, M.I. Din, R. Rehman, A. Akram, S.Z. Ali, Adsorption modeling of alizarin yellow on untreated and treated charcoal, Turkish J. Eng. Environ. Sci. 35 (2011) 209–216.
[44] R. Rehman, A. Abbas, S. Murtaza, J. Anwar, T. Mahmud, S. Akbar, Adsorption parameters optimization for removal of alizarin red-S and brilliant blue FCF dyes from water using Abelmoschus esculentus stem powder, J. Chem. Soc. Pak. 35 (2013) 443–448.
[45] K.M. Joshi, V.S. Shrivastava, Degradation of alizarine red-S (A textiles dye) by photocatalysis using ZnO

and $TiO_2$ as photocatalyst, Int. J. Environ. Sci. 2 (2011) 8–21.
[46] R. Iranpour, J. Zhao, A. Wang, F. Yang, X. Li, Adsorption of alizarin red from aqueous solution using ultrafine fly ash, Adv. Mater. Res. 7 (2012) 518–523.
[47] J. Samusolomon, P.M. Devaprasath, Removal of alizarin red s (dye) from aqueous media by using cynodon dactylon as an adsorbent, J. Chem. Pharm. Res. 5 (2011) 478–490.
[48] D. Li, Q. Liu, S. Ma, Z. Chang, L. Zhang, Adsorption of alizarin red s onto nano-sized silica modified with γ-amino propyl tri ethoxy silane, Adsorpt. Sci. Technol. 29 (2011) 298–300.
[49] H.V. Jadhava, S.M. Khetre, S.R. Bamane, Removal of alizarin red-S from aqueous solution by adsorption on nanocrystalline $Cu_{0.5}Zn_{0.5}Ce_3O_5$, Academic J. (2011) 68–75.
[50] R. Rehman, T. Mahmud, Sorptive elimination of alizarin red-s dye from water using citrullus lanatus-peels in environmentally benign way along with equilibrium data modeling, Asian J. Chem. 25 (2013) 5351–5356.